Self-shading associated with an SBA system for measurement of water-leaving radiance and its correction

ZHEHAI SHANG[1,*], ZHONGPING LEE[1], QIANG DONG[2], JIANWEI WEI[1]

[1]*School for the Environment, University of Massachusetts,Boston, Boston, Massachusetts 02125*
[2]*State Key Lab of Marine Environmental Science, Xiamen University, Xiamen 361005, China*
**Corresponding author: zhehai.shang001@umb.edu*

The shading error associated with the water-leaving radiance (L_w) measured via the Skylight Blocked Approach (SBA, Lee *et al.* 2013) is characterized by Monte Carlo simulations, and it is found this error is in a range of ~1-20% under most water properties and solar positions. A model for estimating this shading error is further developed, and eventually a scheme to correct this error based on the shaded measurements is proposed and evaluated. It is found that the shade-corrected value in the visible domain is within 3% of the true value, which thus indicates that with the SBA scheme, we can obtain not only high precision, but also high accuracy L_w in the field.

OCIS codes: *(280.0280) Remote sensing and sensors; (280.1350) Backscattering; (280.4788) Optical sensing and sensors;*

1. Introduction

Remote-sensing reflectance (R_{rs}, sr^{-1}), defined as the ratio of water-leaving radiance (L_w, $W\ m^{-2}\ sr^{-1}\ nm^{-1}$) to down-welling irradiance just above the surface (E_d, $W\ m^{-2}\ nm^{-1}$), is a key property in optical oceanography, from which a wide range of physical and biogeochemical properties are derived [1]. Separately, the validation of airborne or spaceborne systems for ocean color remote sensing requires accurate measurements of R_{rs} (or L_w) in the field. To achieve this, several approaches have been implemented in the past decades, and the advantages and drawbacks of these are summarized in Mueller *et al.* [2] and Lee *et al.* [3]. These conventional methods generally not measure L_w directly, rather measure some key components and then calculate the desired L_w. The involved post-measurement data processing include removal of surface reflected light, propagation of $L_u(z)$ (vertical profile of upwelling radiance) to L_w, etc., which will bring in considerable uncertainties in the derived L_w and then R_{rs}. The Skylight-Blocked Approach (SBA, Lee *et al.* [3,4]) is a scheme to measure L_w directly, which avoids challenges in dealing with moving clouds or stratified waters and results in L_w with high precision. However, because the radiance sensor looks down while illumination is from above, inevitably there will be shadows from the sensor as well as from the supporting platform [5], which should be corrected for accurate L_w and then R_{rs}.

The shading effect (shading error) in L_w measurement was first discussed in Gordon and Ding [5] (represented as GD92 hereafter in short) for a sensor floating right on the surface. Based on GD92, relative shading error (ε) is defined as

$$\varepsilon = \frac{L_u{}^{true} - L_u{}^{\text{shade}}}{L_u{}^{true}}. \quad (1)$$

$L_u{}^{shaded}$ and $L_u{}^{true}$ are the upwelling radiance just beneath the surface with shading and without shading, respectively. After the transmission through the water-air interface, Eq. (1) could be rewritten as:

$$\varepsilon = \frac{L_w{}^{true} - L_w{}^{measured}}{L_w{}^{true}}, \quad (2)$$

with $L_w{}^{shade}$ and $L_w{}^{true}$ are the water-leaving radiance with shading and without shading, respectively.

Gordon and Ding [5] pointed out that the shading error is a function of the absorption coefficient, the size of the radiometer or the housing, and solar zenith angle at subsurface. They further proposed a simple equation to relate the shading error with the above listed variables as:

$$\varepsilon = 1 - \exp[-\frac{2aR}{\tan(\theta_w)}]. \quad (3)$$

In Eq. (3), θ_w is the subsurface zenith angle of sunlight (accordingly, θ_0 is defined as the zenith angle of sun above surface hereafter), a (m^{-1}) is the absorption coefficient and R (m) is the radius of the sensor or housing. In the years following the studies of Gordon and Ding (1992), shading effects for upwelling irradiance and for sensors 10's of centimeters below the surface were assessed using Monte Carlo (MC) simulations as well [5-9].

SBA is also a floating system different with that evaluated in GD92 [5] and a detailed cartoon of the sensors

and supporting apparatus is presented in Fig. 1.

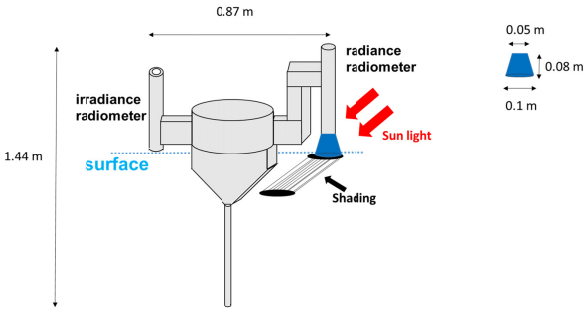

Fig. 1. The SBA system (Lee *et al.*, 2013).

It includes a buoyed platform on the center with radiance and irradiance radiometers attached on both sides. A cone (blue part in Fig. 1) is placed in the front of the radiance radiometer to block surface-reflected light.. Unlike the system addressed by GD92, however, the radiometer employed in an SBA is in air, while it is the cone used to block surface reflected light inserted ~5 cm below the surface. The shading error associated with the SBA system was not adequately addressed, and a first-order correction following GD92 was used in Lee *et al.* [3]. Therefore this study aims to (1) characterize the shading error (ε) associated with the SBA system using MC simulations; and (2) develop an applicable scheme to correct the shading error associated the L_w measurement by an SBA system.

To achieve this, similarly as what was applied in some earlier studies [5,8-10], a backward MC code tracking photon events in waters was developed. Subsequently, L_w^{true} and L_w^{shade} of waters with different optical properties and sun angles were simulated, and ε was further calculated following Eq. (2). After analyzing these ε values, a revised model based on Eq. (3) is developed to express ε as a function of water properties, cone size as well as sun angle. More importantly, an effective scheme is developed to correct this shading error simply from the measured shaded L_w (R_{rs}) spectrum while the pre-knowledge of in-situ IOPs is not required.

2. Monte Carlo approach

The radiative transfer model involved in the MC simulation is detailed in Leathers *et al*. [10]. For each MC simulation of the light field, with and without the presence of the SBA system, it involves the following components and properties:

(1) Optical properties of the water: absorption and scattering coefficients of pure seawater are taken from Lee *et al.* [11], Pope and Fry [12], and Morel [13], respectively. For the IOPs of particles, the absorption and the scattering coefficients were simulated following the "Case-2" model embedded in Hydrolight [14-17] with the concentrations of chlorophyll [Chl, mg m^{-3}] and suspended minerals [SPM, g m^{-3}] as free variables. Contribution of Colored Dissolved Organic Matter (CDOM) is considered co-vary with Chl following Eq.

(4):

$$a_{CDOM}(\lambda) = a_{Chl}(440)\exp[-0.014(\lambda - 440)]. \quad (4)$$

Simulations with a series of Chl and SPM values (as presented in Table 1) were carried out.

The water body is considered as a homogenous medium with infinite depth.

Table 1. selected cases for MC simulation

Case	Chl (mg m^{-3})	SPM (g m^{-3})
1	0.1	0.0
2	1.0	0.0
3	2.0	0.0
4	5.0	0.0
5	5.0	1.0
6	5.0	2.0
7	5.0	5.0

(2) Scattering phase function: three scattering constituents are considered (water molecules, Chl, and SPM). The scattering phase functions of Chl and SPM based on the backscattering ratio of particles [18] were employed. The total scattering phase function is the combined scattering phase function of water molecules, Chl, and SPM.

(3) Downwelling irradiance and light distribution: The total downwelling irradiance above surface ($E_d(0+)$) is set as 1.0 W nm^{-1} m^2. For indirect irradiance, it is assumed that the sky light distribution is isotropic, i.e. idealized sky condition for which the distribution of sky light is independent of the position of sun.

(4) The ratio of indirect irradiance over total irradiance (r_{sky}) is specified in MC input. The 2π space of sky is divided into 217 grids (9 zenith * 24 azimuth + 1 polar grid). After that, radiance in each grid was determined based on r_{sky} and solar position.

(5) Water-air interface: As discussed in Leathers *et al.* [8], the overall impact from wavy surface on shading error is sufficiently small, therefore a flat air-sea interface was considered in this study.

The MC code was written and compiled using Intel Fortran 95 compiler. The MC simulations applied in this effort were backward simulation with its higher efficiency than forward MC simulations. The reliability and confidence of this MC code were evaluated by comparing its radiance outputs under different viewing angle with those from Hydrolight for identical setups when there are no measurement systems, with results showing in Fig. 2.

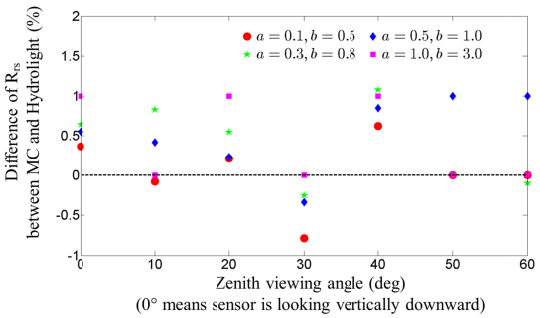

Fig. 2. Comparison between MC results and Hydrolight.

It is found that the difference between radiances from this MC code and that from Hydrolight is generally < 1%, which suggests that the radiance field is reliable from this MC simulation system.

In MC simulations, a shading event is considered when photons hit any part of the sensor or the platform, and the contribution of these photons will be set to 0 when calculating L_w^{shade}.

A further evaluation was carried out to estimate ε of a cylindrical housing sensor on the surface as described in GD92. It is found that the ε values between these two MC simulations for the same ω_0 (single scattering albedo) agree with each other very well (less than 5% relative difference) for $aR < 0.1$ ($R = 0.05$ m) (see Fig. 3).

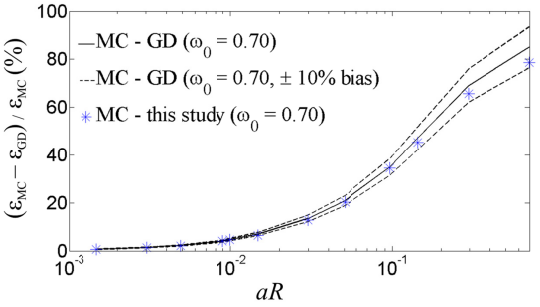

Fig. 3. Comparison of ε between MC results in this work and that in Gordon and Ding when $\theta_0 = 30°$, $R = 0.05$ m.

The dash line represent the 10% bias of result from MC in simulation in Gordon and Ding

For $aR > 0.1$, the impact of (back)scattering effect on shading error becomes more significant and higher difference is observed. But the relative difference is still within 10% ($aR > 0.1$), which provides a validation of the MC code developed here. Note that due to different computer architecture and input setups (i.e., digitization of scattering phase function), there are inherently a few percent of differences in numerically simulated radiance [19], which could explain the higher difference for $aR > 0.1$.

After the MC code was well validated, it was then applied to the present SBA system. To easily represent the structure of the SBA system in our MC code, this complicated structure is decomposed and replaced with a

combination of cylinders (the cone and two radiometers are redrew as a group of cylinders) and cuboids (i.e., supporting platform and rest of the structure) with their measures presented in Fig. 1.

3. Results

3.1 Shading effect of the SBA system

Values of L_w (nadir view) with and without shading of the SBA system were simulated with the MC code for various sun angles and water properties. The shading error due to this SBA system, which is calculated following Eq. (2), can be summarized as follow.

(1) As demonstrated in GD92, there is a strong dependence of ε on sun zenith angle (θ_0) (see Fig. 4). ε increases rapidly from ~10% to more than 40% for θ_0 varied from 60° to 0° (for a = 0.5 m^{-1}, R = 0.05 m).

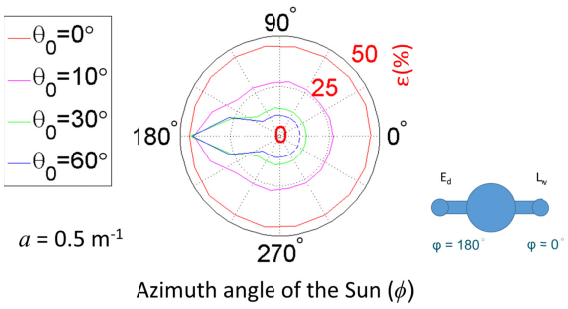

Fig. 4. Shading error of SBA for different solar position.

(2) It appears that the azimuth effect is negligible as long as the radiance sensor of the SBA system is kept with an azimuth angle < 120° (i.e., keep the radiance sensor in the sun side) (see Fig. 4).

(3) The simulation study of GD92 focused on cases dominated by absorption coefficient, where the effect of (back)scattering on this shading effect was omitted. It is found that (back)scattering does have considerable impact on this shading, although it is likely in general secondary. For example, for a = 0.5 m^{-1}, ε changes from 15.7% with b_b/a = 0.15 to 19.5% for b_b/a = 0.30 (see Fig. 5), which is ~20% increase in shading error.

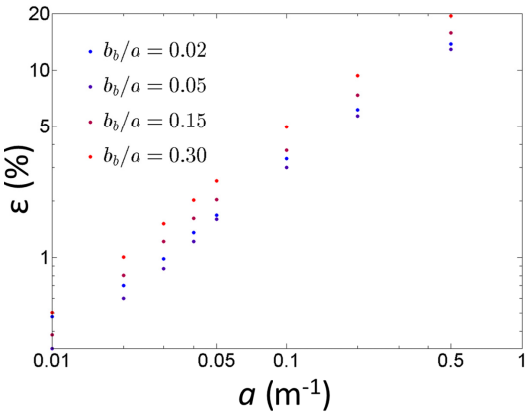

Fig. 5. Variation of shading error with a and b_b; here b =3 x a.

(4) Besides, as presented in Fig. 6, for different θ_0, ε does not monotonously response to an increase of b_b. Shading error decreases with the increase b_b for low b_b values, then increases with an increase b_b. This appears to be a result of the double effects of (back)scattering: a). Water in daytime does not appear as black is simply due to scattering. Therefore, for water with a given absorption coefficient, adding scattering will basically light up the water environment, thus increase the possibility of scattered photons to light up the shaded area by the cone, thus effectively reduce (although might be just slightly) the shading error. b). Backscattering at the same time functions similarly as absorption and effectively reduces the efficiency of photons going forward. Therefore, when b_b increases further, this attenuation effect of light exceeds the illumination gains from backscattered photons and the shading error is increased.

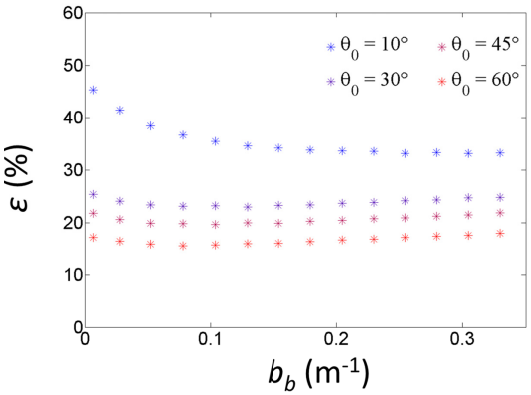

Fig. 6. impact of bb on shading error (ε); a =1 (m-1), b = 8 x a (m-1)

3.2 Modeling the shading error of the SBA system

As a rule of thumb Gordon and Ding [5] described that the shading error is generally a function of waters' absorption coefficient, where the effect of (back)scattering is omitted. This is applicable for waters or wavelengths where absorption coefficient dominates. However, for waters or wavelengths where scattering are significant due to extremely high concentration of Chl and/or SPM, such as many coastal and inland waters, it is necessary to include the effect due to scattering. We therefore developed a more general model aimed for applications for both clean oceanic water and coastal waters with strong (back)scattering effect.

Following GD92, a general formula for the shading error is described as:

$$\varepsilon = 1 - \exp\left[-\left(K_{L_u} + K_L\right)\frac{R}{tan(\theta_w)}\right], \tag{5}$$

where K_{L_u} (m^{-1}) is the attenuation coefficient of upwelling radiance (nadir view or zenith going) under no shade and K_L (m^{-1}) is the attenuation coefficient for upwelling radiance in the shade. In this study, the radius of the cone (as presented in Fig. 1, about 0.05 m) is taken to be the value of R.

Following descriptions of the diffuse attenuation coefficient of downwelling irradiance [20], we may consider both K_{L_u} and K_L as functions of a and b_b as well as solar zenith angle at subsurface, and represent the sum of K_{L_u} and K_L as K. K can then in general be described as:

$$K = f_1(a, b_b, \theta_w). \tag{6}$$

Further, by least-square fitting of the ε data obtained from MC simulations for the wide range of IOPs and three sun angles, we obtained an empirical formula for K as:

$$K(\lambda) = [3.15\sin(\theta_w) + 1.15]\mathrm{e}^{-1.57b_b(\lambda)}\,a(\lambda) + [5.62\sin(\theta_w) - 0.23]\mathrm{e}^{-0.5a(\lambda)}b_b(\lambda). \tag{7}$$

The estimated ε based on the above K model for θ_0 = 10°, 30° and 60° is compared with that simulated by MC (see Fig. 7), where an overall average error of 5.8% is obtained. Also shown is the estimation of ε based on the formula of Gordon and Ding [5], where an overall average error of 38.1% is found for this dataset, likely a result of omitting the effect of (back)scattering in the model of GD92.

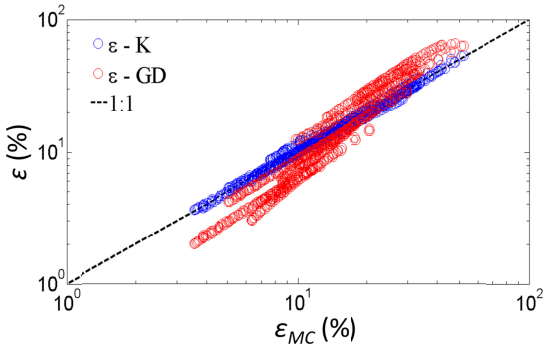

Fig. 7. Estimated ε through K (Eqs. (5) and (7)) and Gordon and Ding (y-axis) .VS. calculated ε from MC (x-axis).

Note that in the above evaluations and later on shading error corrections, the azimuth angle of the radiance sensor (ϕ) is set at 0° (as the coordinate system present in Fig. 4), since the impact of azimuth angle on the shading effect (as long as ϕ is kept < 120° from the sun plane) is negligible.

3.3 Correction of shading error

3.3.1 Overall scheme of shading correction

An imperative step in the L_w measurement by SBA (and other in-water measurements) is to correct the shading error due to the system. As shown in Gordon and Ding's study [5] and the above, this error depends on IOPs, sun angle as well as the size of the radiometer. Although the latter two can be known for any given measurement system and time and location, the IOPs are not handily available at the time of measuring L_w. Here we present an effective scheme to derive IOPs from the shaded L_w, and then use this IOP products to correct the shading error.

Let's define a remote-sensing reflectance under the shading effect as

$$R_{rs}{}^{shade} = \frac{L_w{}^{shade}}{E_d(0+)}. \tag{8}$$

This $R_{rs}{}^{shade}$ can then be related to the desired no-shade R_{rs} ($R_{rs}{}^{true}$) as:

$$R_{rs}{}^{shade} = R_{rs}{}^{true}(1-\varepsilon). \tag{9}$$

Decades of studies [21,22] have found that $R_{rs}{}^{true}$ can be modeled as a function of IOPs through

$$R_{rs}{}^{true}(\lambda) = \frac{0.52 r_{rs}(\lambda)}{1-1.7 r_{rs}(\lambda)}, \tag{10}$$

with r_{rs} the remote sensing reflectance right below the surface and can be expressed as that shown in Lee *et al.* [23],

$$r_{rs}(\lambda) = g_w \frac{b_{bw}(\lambda)}{a(\lambda)+b_b(\lambda)} + g_p \frac{b_{bp}(\lambda)}{a(\lambda)+b_b(\lambda)}, \tag{11}$$

$$g_p(\lambda) = G_0\{1 - G_1 \exp\left[-G_2 \frac{b_{bp}(\lambda)}{a(\lambda)+b_b(\lambda)}\right]\}. \tag{12}$$

Here g_w and g_p are two model parameters for molecular scattering and particle scattering phase functions, respectively, while values of G_0, G_1, and G_2 are constants for given light geometry and particle phase function [22]. Since ε is also a function of the absorption and backscattering coefficients (Eqs. (5)-(7)), the above models indicate that $R_{rs}{}^{shade}$ is simply also a function of IOPs, therefore we may derive these IOPs from $R_{rs}{}^{shade}$ spectrum similarly as that to derive IOPs from no-shade R_{rs}.

We adopted the hyperspectral optimization processing exemplar (HOPE) described in Lee *et al*. [24] for this derivation. Briefly, a and b_b are modeled as:

$$a(\lambda) = a_w(\lambda) + a_{ph}(\lambda) + a_{dg}(\lambda), \tag{13}$$

$$b_b(\lambda) = b_{bw}(\lambda) + b_{bp}(\lambda). \quad (14)$$

Here a_w and b_{bw} are the absorption and backscattering coefficient of pure seawater with same values used for MC simulation in this study. a_{ph} and a_{dg} are the absorption coefficient of phytoplankton and detritus and CDOM, respectively; b_{bp} is the back scattering coefficient of particles. a_{ph}, a_{dg} and b_{bp} spectra are further modeled, respectively, as [24-26]:

$$a_{ph}(\lambda) = [a_0(\lambda) + a_1(\lambda)\ln(P)]P, \quad (15)$$

$$a_{dg}(\lambda) = G\exp\left[S_{dg}(440 - \lambda)\right], \quad (16)$$

$$b_{b_p}(\lambda) = \left(\frac{440}{\lambda}\right)^{\eta} b_{b_p}(440), \quad (17)$$

In which, a_0 and a_1 are model constants presented in Lee [27], S_{dg} is the slope of a_{dg}. P, G, η and $b_{bp}(440)$, which represent $a_{ph}(440)$, $a_{dg}(440)$, slope of b_{bp} and particle backscattering at 440 nm, are four free variables to model R_{rs}^{shade}. To improve the performance of this scheme, an initial guess of η (η_{ini}) was determined as in QAA version 6 (QAA_v6) [28] without considering shading error at both 440 nm and 555 nm:

$$\eta_{ini} = 2.0\{1 - 1.2\exp[-0.9\frac{r_{rs}(440)}{r_{rs}(555)}]\}. \quad (18)$$

$$r_{rs}(\lambda) = \frac{R_{rs}^{shade}(\lambda)}{0.52+1.7R_{rs}^{shade}(\lambda)}. \quad (19)$$

Where R_{rs}^{shade} is the in-situ R_{rs} (or R_{rs}^{shade} from MC simulation). The upper and lower boundary of variation range of η is set as $0.5*\eta_{ini}$ and $1.5*\eta_{ini}$, respectively.

To estimate the value of S_{dg}, a referenced band at 555 nm is chosen with its relative low shading error (normally less than 10%) and strong signal for most cases. Based on Eq. (19), neglect of shading error will result less than 10% error on estimation of $r_{rs}(555)$, which has limited impact on estimation of S_{dg} (about 5%). With this neglect of shading error at 555nm, from Eq. (19), we have value of $r_{rs}(555)$ calculated as:

$$r_{rs}(555) = \frac{R_{rs}^{shade}(555)}{0.52+1.7R_{rs}^{shade}(555)}. \quad (20)$$

While at the same time, from Eq. (11), $r_{rs}(555)$ is a function of IOPs at 555nm as well:

$$r_{rs}(555) = g_w\frac{b_{bw}(555)}{a(555)+b_b(555)} + g_p\frac{b_{bp}(555)}{a(555)+b_b(555)}, \quad (21)$$

From Eqs. (14)-(15) and (17), $r_{rs}(555)$ could be expressed as:

$$r_{rs}(555) = f_2\left(P, G, b_{bp}(440), \eta, S_{dg}\right). \quad (22)$$

Since value of $r_{rs}(555)$ is known and calculated from Eq. (20), Eq. (22) could be rewritten as:

$$S_{dg} = f_3\left(P, G, b_{bp}(440), \eta\right). \quad (23)$$

Consequently, R_{rs}^{shade} becomes a function of four free variables P, G, η and $b_{bp}(440)$ which could be derived numerically through spectral optimization (Huang *et al*., Werdell *et al*.) [29,30].

The error function for the spectral optimization is defined as:

$$Err = \frac{\{average(\lambda = 400 - 750\ nm)[R_{rs}{}^{shade\_mod}(\lambda) - R_{rs}{}^{shade}(\lambda)]^2\}^{0.5}}{average(\lambda = 400 - 750\ nm)[R_{rs}{}^{shade}(\lambda)]} \quad (24)$$

Where $R_{rs}{}^{shade\_mod}$ is the modeled shading R_{rs} estimated through Eqs. (9)-(17), $R_{rs}{}^{shade}$ is the in-situ R_{rs} (or $R_{rs}{}^{shade}$ get from MC simulation). Subsequently ε was estimated based on the derived IOPs (Eqs. (5)-(7)). Further, from Eq. (9), the shading-corrected R_{rs} ($R_{rs}{}^{correct}$) became:

$$R_{rs}{}^{correct}(\lambda) = \frac{R_{rs}{}^{shade}(\lambda)}{(1 - \varepsilon(\lambda))}. \quad (25)$$

3.3.2 **Evaluation of the shading-correction scheme**

To characterize the difference between the derived value (i.e., $R_{rs}{}^{correct}$, derived IOPs) and the true value (i.e., $R_{rs}{}^{true}$, input IOPs in MC simulation or IOPs in real world), *NRMSE* (normalized root-mean-square error) is employed:

$$NRMSE = \sqrt{\frac{\sum_{i=1}^{n}(\hat{y}_i - y_i)^2}{n}}\frac{1}{\bar{y}}, \quad (26)$$

where $\hat{y}_i$ and y_i are the predicted and the true value of a property (e.g., R_{rs}), respectively, and $\bar{y}$ is the average of the true value.

Examples of $R_{rs}{}^{correct}$ spectra for different Chl and SPM values obtained from the above processes, along with its comparison with $R_{rs}{}^{true}$ spectra for θ_0 = 10°, 30°, and 60°, are presented in Figs. 8 and 9. It is found in general the *NRMSE* between $R_{rs}{}^{correct}$ and $R_{rs}{}^{true}$ is under 2% for these low and high Chl and SPM waters, and for θ_0 from 10° to 60°, respectively. Larger (> 15%) difference is found for wavelengths beyond 720 nm and for θ_0 as 10° (as shown in Fig. 8), a result of R_{rs} with high absorption (> 1.2 m^{-1}) and under intense self-shading (> 40%, 28%, 20% when θ_0 = 10°, 30°, 60°, respectively). For such scenarios, the accuracy of R_{rs} is not that valuable as its application in ocean color remote sensing is limited. Separately, from Fig. 8, about 10% relative difference of ε is found in blue bands (λ = 400 – 440 nm) for several cases (Chl = 5.0 mg m^{-3}, SPM = 0.0, 1.0 and 5.0 g m^{-3} when θ_0 = 10°). These are simply due to a mismatch between the power-law model (Eq. (17)) used to describe the b_{bp} spectrum did not match the b_{bp} spectrum used in MC simulations. Consequently, larger errors in the retrieved IOPs were resulted, which then propagates to the estimation of ε. Nevertheless, even with such conditions, on average the resulted $R_{rs}{}^{correct}$ (λ = 400 – 720 nm) is still within 3% (3%, 1.5%, 1% when θ_0 = 10°, 30°, 60°, respectively) of $R_{rs}{}^{true}$, which suggests a successful removal of the shading effects, at least for cases studied here.

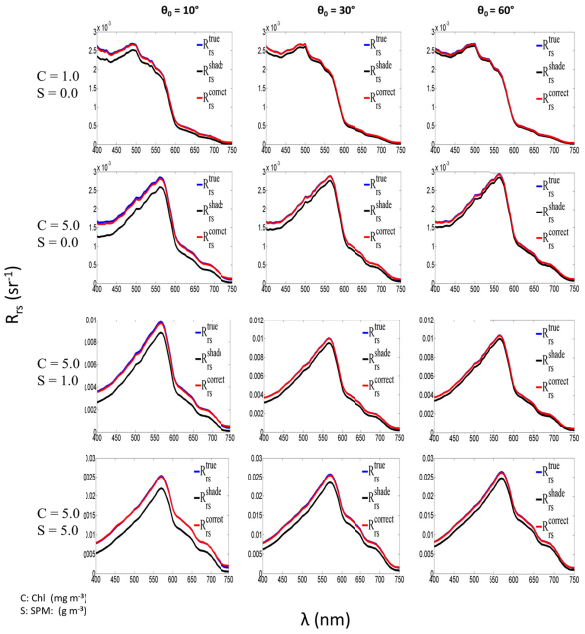

Fig. 8. Comparison between shaded-corrected R_{rs} and true R_{rs} generated from MC.

Blue: true R_{rs} generated from MC; Red: shaded-corrected R_{rs}; Black: shaded R_{rs} generated from MC

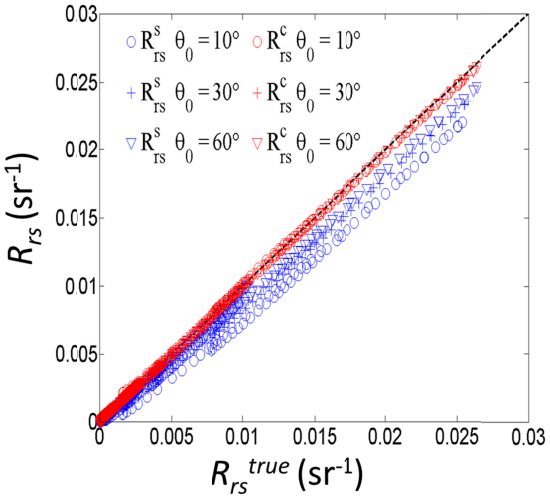

Fig. 9. Comparison between shaded-corrected R_{rs} and true R_{rs} generated from MC.

R_{rs}^{s}: shaded R_{rs}; R_{rs}^{c}: shaded-corrected R_{rs}; R_{rs}^{true}: true R_{rs}, get from MC simulation

4. Discussion

4.1 Impact of inaccurate IOPs on the shading correction

The optimization scheme results in spectra of a and b_b with least Err between R_{rs}^{shade} and $R_{rs}^{shade\_mod}$. However,

least *Err* for R_{rs} does not guarantee the best match between the real IOPs (here refer to the IOPs used in MC simulations) and the retrieved IOPs. As shown in Figs. 10(a), 10(b) and 11, inconsistent estimations of both a and b_b are found.

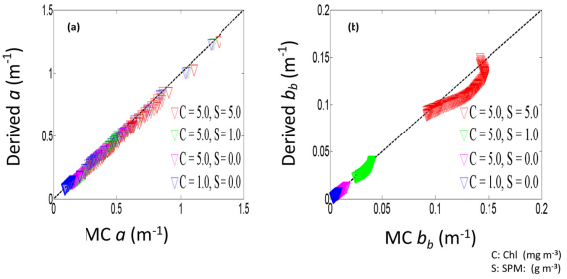

Fig. 10. Derived IOPs from New model .VS. Input IOPs in MC.

In this effort, the *NRMSE* of derived IOPs are on average about 6.6% for a and 10.6% for b_b. As mentioned above, the errors of derived IOPs are mainly due to mismatches between the IOPs spectral models (Eqs. (15) - (17)) and the IOPs spectra used in MC simulations. Table 2 presents the *NRMSE* of derived IOPs and corrected R_{rs} for four representative cases.

Table 2. *NRMSE* of derived IOPs and corrected R_{rs}

Cases	Derived a	Derived b_b	Corrected R_{rs}
C = 1.0, S = 0.0	2.0%	2.7%	0.9%
C = 5.0, S = 0.0	3.7%	9.2%	1.6%
C = 5.0, S = 1.0	4.7%	9.2%	1.4%
C = 5.0, S = 5.0	6.6%	10.6%	1.3%
Overall of the 4 cases above	5.2%	15.9%	1.8%

C: Chl (mg m^{-3})
S: SPM (g m^{-3})

Much higher *NRMSE* is found for derived IOPs in the case Chl = 5.0 mg m^{-3}, SPM = 1.0 g m^{-3}. For this case, a significant mismatch in spectral shape of backscattering coefficient is observed in the green bands (490-600 nm) (Fig. 11) and result an underestimation of b_{bp}. Consequently, to compensate this overestimation, higher absorption coefficient than true values will be derived as shown in Fig. 11. However, with this mismatch of derived IOPs, the *NRMSE* of R_{rs} in this case remains at an excellent level (< 2%). This is because, with the current SBA physical size (radius of the cone is about 5 cm), for $a(440)$ = 0.5 m^{-1} and $b_b(440)$ = 0.05 m^{-1} (values that cover > 90% of global oceans), a 10% error in $a(440)$ and $b_b(440)$ will only result in less than 3%, 2%, 1% relative difference in R_{rs} for θ_0 = 10°, 30°, and 60°, respectively. This indicates that, for a radius of the cone at 5 cm, for most water body in the world, the inaccuracy in derived IOPs will only bring limit impact on shading correction.

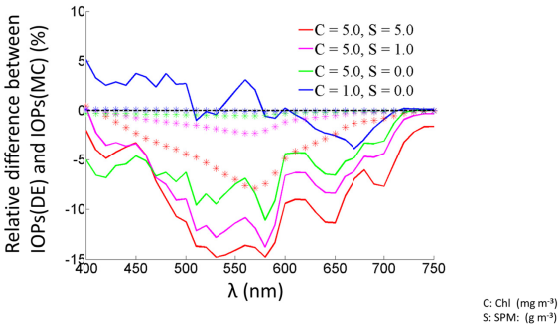

Fig. 11. Derived a and bb .VS. MC input a and b_b when $\theta_0 = 30°$

MC: MC input; DE: Derived; Solid line: absorption; Star: backscattering

4.2 Sensitivity of ε to R

Based on Eq. (5), ε is a function of IOPs, θ_0 and R. IOPs are aquatic parameters decided by nature. Obviously (see Table 3), the smaller the R, the less the shading effect and the less error that may be brought in from shading correction. For θ_0, due to various limitation in field measurements (matching up with satellite or cruise schedule etc.), it is a parameter that cannot be pre-determined. R depends on the design of the SBA system, which is the only parameter that can be "manipulated" at the system manufacture stage. Table 3 shows the range of ε for a few value of R. For the present SBA system, for R as 5 cm, at $\theta_0 = 30°$, ε decreases from 11.7% to 1.2% with K decrease from 1.0 m^{-1} to 0.1 m^{-1}. If R could be reduced, say to 2 cm, for the same conditions, ε changes from 4.9% to 0.5% (see Table 3).

Table 3. Shading error (ε) under different K value and radius (R) of sensor when solar zenith (θ_0) = 30°

$\theta_0 = 30°$	ε (%)		
R (m)	K = 0.1 (m^{-1})	K = 0.5 (m^{-1})	K = 1.0 (m^{-1})
0.01	0.25	1.24	2.46
0.02	0.50	2.46	4.85
0.03	0.74	3.66	7.19
0.04	0.99	4.85	9.47
0.05	1.24	6.03	11.70
0.06	1.48	7.19	13.87
0.07	1.73	8.34	15.98
0.08	1.97	9.47	18.05
0.09	2.21	10.59	20.06
0.10	2.46	11.70	22.02

In particular, if R can be kept at 3 cm or smaller, the shading error is generally less than 7.2% even for K is as high as 1.0 m^{-1} when $\theta_0 = 10°$ (a and b_b are about 0.5 m^{-1} and 0.05 m^{-1}, respectively). Also, if applying to the most turbid case (Chl = 5.0 mg m^{-3}, SPM = 5.0 g m^{-3}; corresponding a = 0.66 m^{-1} and b_b = 0.15 m^{-1}) in the MC simulation as another example, for solar zenith angle varies from 10° to 60°, reducing R from 5 cm to 2 cm will

cut more than half of the shading error (see Table 4). These results indicate high confidence in precisely and accurately measuring L_w in the field in the 350-720 nm range if an SBA system can be manufactured with a small-sized radiometer.

Table 4. Shading error (ε) at 440 nm for case Chl = 5.0 (mg m^{-3}), SPM = 5.0 (g m^{-3}) under different radius (R) of the cone

	ε (%)		
R (m)	$\theta_0 = 10°$	$\theta_0 = 30°$	$\theta_0 = 60°$
0.01	6.44	3.46	2.65
0.02	12.47	6.80	5.24
0.03	18.11	10.03	7.75
0.04	23.39	13.14	10.20
0.05	28.32	16.15	12.59
0.06	32.94	19.05	14.91
0.07	37.26	21.85	17.16
0.08	41.30	24.56	19.36
0.09	45.08	27.17	21.50
0.10	48.62	29.69	23.59

5. Conclusions

In ocean color remote sensing, to achieve precise and accurate measurement of L_w (R_{rs}) in-situ has been a long elusive goal. The above-water approach runs into the difficulty to remove surface-reflected light, while the in-water systems suffer shading errors and associated with the uncertainties of manually propagating upwelling radiance to L_w. The SBA system does measure L_w directly with high precisions, but, inevitably, there are self-shading errors associated with such measurements. Here, following the approach of Gordon and Ding [5], we characterized the shading errors for various optical properties, sun angles, and size structure using Monte Carlo simulations. It is found that depends on values of these parameters, the shading error can change from negligible to more than 20% in most cases. We further revised the model of GD92 [5] to include the effects of backscattering for the shading effect. More importantly, a practical scheme is developed to correct the shading effect simply based on the measured, shaded, L_w (R_{rs}). The resulted, shading-corrected, R_{rs} is found generally within 2% of the true (without shading) R_{rs}. These results indicate that, with the SBA concept and the correction scheme, we can now not only obtain R_{rs} with high precision, but with high accuracy. However, as indicated in Lee *et al.* [3], the ultimate, by-passing sophisticated post-measurement processing, solution for high-precision and high-accuracy R_{rs} is to manufacture an SBA system with a small-sized radiometer for radiance.

Acknowledgment

Support for this study was provided by NASA. The authors very appreciate the Massachusetts Green High Performance Computing Cluster to provide resources for running a great number of simulations.

Appendix: IOPs of each components for MC simulations

Similar as the Hydrolight "Case-2" model setting, the IOPs input for MC simulations are divided into four parts: pure water, chlorophyll, CDOM and SPM.

As mentioned previously, the IOPs of pure water are taken from Lee *et al.* [11], Pope and Fry [12], and Morel [13], respectively. For the other three constituents, the same models as those embedded in Hydrolight are applied.

The IOPs of Chl is estimated by:

$$a_{chl}(\lambda) = a^*(\lambda)[CHL]^{0.65} \text{ [17]}, \tag{27}$$

$$b_{chl}(\lambda) = 0.3a^*(\lambda)[CHL](\frac{555}{\lambda})^{0.62} \text{ [15]}. \tag{28}$$

Where [CHL] is the concentration of chlorophyll (mg m^{-3}). A backscattering ratio of 0.01 is assign to chlorophyll.

For CDOM, the absorption is calculated as presented in Eq. (4).

For SPM, the IOPs is determined by:

$$a_{SPM}(\lambda) = a^*_{SPM}(\lambda)[SPM], \tag{29}$$

$$b_{SPM}(\lambda) = b^*_{SPM}(\lambda)[SPM]. \tag{30}$$

Where [SPM] is the concentration of SPM in (g m^{-3}). The value of a^*_{SPM} and b^*_{SPM} is taken from average specific particle absorption and scattering in Hydrolight, which could be retrieved from "HE5/data/defaults/astarmin_average.txt", "HE5/data/defaults/bstarmin_average.txt", respectively. A backscattering ratio of 0.03 is assigned to SPM.

The volume scattering function will be constructed based on the back scattering ratio [18].

Reference

1. C. R. McClain, "A decade of satellite ocean color observations*," Annual Review of Marine Science **1**, 19-42 (2009).
2. J. L. Mueller, G. S. Fargion, C. R. McClain, S. Pegau, J. Zanefeld, B. G. Mitchell, M. Kahru, J. Wieland, and M. Stramska, "Ocean optics protocols for satellite ocean color sensor validation, revision 4, volume IV: Inherent optical properties: Instruments, characterizations, field measurements and data analysis protocols," (2003).
3. Z. Lee, N. Pahlevan, Y.-H. Ahn, S. Greb, and D. O'Donnell, "Robust approach to directly measuring water-leaving radiance in the field," Appl. Opt. **52**, 1693-1701 (2013).
4. A. Tanaka, H. Sasaki, and J. Ishizaka, "Alternative measuring method for water-leaving radiance using a radiance sensor with a domed cover," OExpr **14**, 3099-3105 (2006).
5. H. R. Gordon, and K. Ding, "Self-shading of in-water optical instruments," Limnol. Oceanogr **37**, 491-500 (1992).
6. J. Piskozub, "Effects of surface waves and sea bottom on self-shading of in-water optical instruments," in *Ocean Optics XII*(International Society for Optics and Photonics1994), pp. 300-308.
7. J. Piskozub, A. R. Weeks, J. N. Schwarz, and I. S. Robinson, "Self-shading of upwelling irradiance for an instrument with sensors on a sidearm," Appl. Opt. **39**, 1872-1878 (2000).
8. R. Leathers, T. V. Downes, and C. Mobley, "Self-shading correction for upwelling sea-surface radiance measurements made with buoyed instruments," OExpr **8**, 561-570 (2001).
9. R. Leathers, T. Downes, and C. Mobley, "Self-shading correction for oceanographic upwelling radiometers," OExpr **12**, 4709-4718 (2004).
10. R. A. Leathers, T. V. Downes, C. O. Davis, and C. D. Mobley, "Monte Carlo radiative transfer simulations for ocean optics: a practical guide," (DTIC Document, 2004).
11. Z. Lee, J. Wei, K. Voss, M. Lewis, A. Bricaud, and Y. Huot, "Hyperspectral absorption coefficient of "pure" seawater in the range of 350–550 nm inverted from remote sensing reflectance," Appl. Opt. **54**, 546-558 (2015).
12. R. M. Pope, and E. S. Fry, "Absorption spectrum (380–700 nm) of pure water. II. Integrating cavity measurements," Appl. Opt. **36**, 8710-8723 (1997).

13. A. Morel, "Optical properties of pure water and pure sea water," Optical aspects of oceanography **1**, 1-24 (1974).
14. C. D. Mobley, and L. K. Sundman, "HYDROLIGHT 5 ECOLIGHT 5," (2008).
15. H. Gordon, A. Morel, R. Barber, N. Mooers, M. Bowman, and B. Zeitzschel, "A Review Lecture Notes on Coastal and Estuarine Studies," in *Remote Assessment of Ocean Color for Interpretation of Satellite Visible Imagery*(Springer-Verlag NY, 1983).
16. A. Morel, "Light and marine photosynthesis: a spectral model with geochemical and climatological implications," Prog. Oceanogr. **26**, 263-306 (1991).
17. A. Morel, "Optical modeling of the upper ocean in relation to its biogenous matter content(Case I waters)," J. Geophys. Res. **93**, 749-710 (1988).
18. G. R. Fournier, and M. Jonasz, "Computer-based underwater imaging analysis," in *SPIE's International Symposium on Optical Science, Engineering, and Instrumentation*(International Society for Optics and Photonics1999), pp. 62-70.
19. C. D. Mobley, B. Gentili, H. R. Gordon, Z. Jin, G. W. Kattawar, A. Morel, P. Reinersman, K. Stamnes, and R. H. Stavn, "Comparison of numerical models for computing underwater light fields," Appl. Opt. **32**, 7484-7504 (1993).
20. Z. P. Lee, K. P. Du, and R. Arnone, "A model for the diffuse attenuation coefficient of downwelling irradiance," Journal of Geophysical Research: Oceans **110** (2005).
21. H. R. Gordon, O. B. Brown, R. H. Evans, J. W. Brown, R. C. Smith, K. S. Baker, and D. K. Clark, "A semianalytic radiance model of ocean color," Journal of Geophysical Research: Atmospheres **93**, 10909-10924 (1988).
22. Z. Lee, K. L. Carder, and R. A. Arnone, "Deriving inherent optical properties from water color: a multiband quasi-analytical algorithm for optically deep waters," Appl. Opt. **41**, 5755-5772 (2002).
23. Z. Lee, K. L. Carder, and K. Du, "Effects of molecular and particle scatterings on the model parameter for remote-sensing reflectance," Appl. Opt. **43**, 4957-4964 (2004).
24. Z. Lee, Y.-H. Ahn, C. Mobley, and R. Arnone, "Removal of surface-reflected light for the measurement of remote-sensing reflectance from an above-surface platform," OExpr **18**, 26313-26324 (2010).
25. Z. Lee, K. L. Carder, C. D. Mobley, R. G. Steward, and J. S. Patch, "Hyperspectral remote sensing for shallow waters. I. A semianalytical model," Appl. Opt. **37**, 6329-6338 (1998).
26. Z. Lee, K. L. Carder, C. D. Mobley, R. G. Steward, and J. S. Patch, "Hyperspectral remote sensing for shallow waters: 2. Deriving bottom depths and water properties by optimization," Appl. Opt. **38**, 3831-3843 (1999).
27. Z. Lee, "VISIBLE-INFRARED REMOTE-SENSING MODEL," (University of South Florida, 1994).
28. IOCCG, "QAA_v6," http://www.ioccg.org/groups/Software_OCA/QAA_v6_2014209.pdf.
29. P. J. Werdell, B. A. Franz, S. W. Bailey, G. C. Feldman, E. Boss, V. E. Brando, M. Dowell, T. Hirata, S. J. Lavender, Z. Lee, H. Loisel, S. Maritorena, F. Mélin, T. S. Moore, T. J. Smyth, D. Antoine, E. Devred, O. H. F. d'Andon, and A. Mangin, "Generalized ocean color inversion model for retrieving marine inherent optical properties," Appl. Opt. **52**, 2019-2037 (2013).
30. S. Huang, Y. Li, S. Shang, and S. Shang, "Impact of computational methods and spectral models on the retrieval of optical properties via spectral optimization," OExpr **21**, 6257-6273 (2013).